Sensorless Commissioning of Synchronous Reluctance Machines Augmented with High Frequency Voltage Injection

Sensorless Commissioning of Synchronous Reluctance Machines Augmented with High Frequency Voltage Injection

Paolo Pescetto, Gianmario Pellegrino
Politecnico di Torino, Energy department
Corso Duca degli Abruzzi 24, Torino, Italy
paolo.pescetto@polito.it

***Abstract*—This paper deals with the self-commissioning of synchronous reluctance motors. Previous work has demonstrated that the motor flux maps can be accurately identified at standstill by exciting the machine with square-wave voltage pulses of large amplitude, of the same order of the machine nominal voltage. This was made without the need of rotor locking and without using position sensors. The knowledge of the *d* and *q* axes position was obtained by a preliminary sensorless commissioning and then used for directing the *d* and *q* voltage pulses accordingly, in open-loop fashion. At free shaft, the position tends to oscillate under such alternated excitation, introducing position error and thus inaccuracy. For high values of the torque current component i_q the rotor can even start spinning suddenly, thus stopping the identification. The loss of control impedes of identification of the flux maps above a certain limit, at least in the *q* direction. In the past, polynomial fitting was used to extrapolate the flux map in the missing parts of the *dq* current domain, with good results. In this paper, the rotor position is closed-loop estimated during the motor commissioning, so to counteract the occurrence of sudden spin and extend the explored current area in the q direction. An additional pulsating voltage, also of the square-wave type, is superimposed to the main excitation voltage, and the position is tracked through current demodulation. In this way, the area explored in the *dq* current plane is substantially extended, if compared to previous method. The proposed approach is verified through experimental results on one synchronous reluctance motor prototype.**

Keywords—Magnetic Model Identification; Self-Commissioning; Synchronous Reluctance Motor; Flux Maps; Magnetization Curves; HF injection

I. INTRODUCTION

The adoption of Synchronous Reluctance motor drives (SyRM) for industry applications is considerably growing, mainly due to their high efficiency and competitive torque per volume ratio. In many industry applications, sensorless operation is very welcome. The literature offers different solutions for sensorless control of the SyRM [1][2], but all of them require the knowledge of the current-to-flux machine characteristics, at least for the zero-speed operating region. This is a demanding issue due to the relatively complex magnetic structure of SyRMs, resulting in highly non-linear saturation and cross-saturation characteristic.

The constant speed test in [3] can be considered the state of the art in terms of accurate identification of the SyRM flux maps. However, this constant speed test requires a dedicated test rig and a position transducer, and it is therefore not compatible with the full-sensorless approach. In recent years, several automatic self-commissioning techniques have been proposed for synchronous motor drives [4]-[8]. Yet, most of them require additional hardware and a position transducer.

Square-wave voltage excitation at standstill was first proposed in [9] using pulses of low per unit value, for interior permanent magnet machines having a position transducer, and with the rotor locked. More recently [10][11], the technique was improved specifically for SyR machines, with the introduction of high test voltages and sensorless implementation. The identification is performed at standstill and free-shaft, which is the worst-case condition for standstill self-commissioning, demonstrating to be accurate and robust towards stator resistance detuning. Plus, it is encoderless. In [10][11], the rotor position is off-line estimated before the test through high frequency (HF) signal injection and demodulation, or determined via initial parking through DC excitation, and then considered constant during the test. In turn, any unwilled movement of the rotor provoked by the machine response to the excitation of [10][11] would make the initial position estimation inaccurate, to the point that the rotor would even start spinning and the test would fail. This shortcoming limits the feasible measurement area in the *dq* current plane. The identification technique was further improved in [12] with the introduction of an automatic tuning procedure, according to which the test can be stopped before failing most of the times, and data collected before one test failure can be used for curve fitting anyway.

In this work, HF voltage injection is used to online estimate the rotor position during the flux map identification. In this way, the *dq* axes position is tracked in real time, considerably reducing the risk of rotor movement and test failure. The augmented identification method can increase the area explored in the *dq* current plane, respect to the previous version with open-loop position estimation. Moreover, the test is more stable than before, permitting to acquire a higher number of points, in a larger area of exploration. The paper provides a detailed theoretical analysis, supported by experimental validation on a 2.2 kW SyRM prototype.

II. Review of the Self-Commissioning Method

During the self-commissioning, the motor shaft is free. There is no position transducer, the angular position of the *d* axis is estimated. The motor currents are measured and the voltages are estimated via the inverter voltage commands, indicated with a star superscript. The flux maps commissioning procedure is divided into three steps, referring to the exploration of the *d*, *q*, and *d*+*q* axes curves, respectively.

In **test #1**: the *d* axis is excited with a bipolar square-wave voltage v_d^*, reversing its polarity whenever the absolute value of i_d overcomes a defined threshold value $i_{d,max}$. Meanwhile, v_q^* is set to 0. In this way, the *d* axis magnetic characteristic $\hat{\lambda}_d(i_d, i_q = 0)$ is evaluated as:

$$\hat{\lambda}_d = \int \left(v_d^* - \hat{R}_s i_d\right) dt \tag{1}$$

where $\hat{R}_S$ is the stator resistance estimate. Both $\hat{R}_S$ and the inverter actuation error can be measured off-line before the test through one of the several self-commissioning methods, e.g. [8]. In **test #2** the same procedure is repeated for the *q*-axis, with $v_d^* = 0$, to evaluate $\hat{\lambda}_q(i_d = 0, i_q)$ in the imposed range $i_{q,max}$.

$$\hat{\lambda}_q = \int \left(v_q^* - \hat{R}_s i_q\right) dt \tag{2}$$

During **test #3** both the axes are excited at the same time, and each voltage component reverses according to the respective current limit. Equations (1) and (2) are used also in this test, for completing the exploration and identification of the flux maps $\hat{\lambda}_d(i_d, i_q)$ and $\hat{\lambda}_q(i_d, i_q)$ in the current regions out of the i_d and i_q axes. The amplitude of the test square wave voltage in d and q axes are called $V_{test,d}$ and $V_{test,q}$, respectively. Details can be found in [11].

In previous works [10]-[12], the initial position of the rotor is evaluated only once before starting the test, either using a saliency based sensorless technique (e.g. pulsating or rotating high frequency voltage injection) or by imposing the rotor position exciting the machine with direct current (rotor parking). It was thus assumed that such initial position was maintained while the flux curves were identified using the initially estimated *dq* coordinates.

A. Open loop and closed loop approaches

In principle, tests #1 and #2 do not produce transient torque, because only one axes is excited at a time, which means zero torque produced. In practice, this is true for Test #1 but not for Test #2. The *d* test is highly stable, as eventual rotor misalignments produce a stabilizing torque that tends to align the rotor to the real *d* axis. The *q* test is only marginally stable, as when the voltage is injected on the wrong $\hat{q}$ direction, the torque output tends to further increase the misalignment. Test #3 involves non zero alternated torque that continuously reverses its sign and tends to be null in average.

In a well conducted identification, the rotor should vibrate around its initial position without significant average misalignments. For practical implementation though, any rotor misalignment must be taken into account.

Therefore, test #1 will be performed as in [11], using the initial off-line estimation of the rotor position. Test #2 and Test #3 will be assisted by online sensorless position estimation to extend the feasible current limit $i_{q,max}$ *and* extend the measurement domain in the current plane i_d, i_q.

As suggested in [12], the $i_{q,max}$ limit used in the hysteresis control of tests #2 and #3 is progressively increased starting from zero, and the test is automatically stopped when a relevant position error is detected.

B. Stop criteria

Test #2 uses the amplitude of the $\hat{d}$ axis current as an error feedback, as proposed in [12], and stops the identification when this component reaches a predetermined threshold.

Conversely, the technique proposed in [12] for test #3 is based on the derivative of i_d and does not apply when in presence of HF injection, because the HF component distorts the waveform of i_d. Therefore, at this stage of the investigation, even if the position estimation used in the control is completely sensorless, an encoder was used to detect rotor movement and stop the *dq* test#3.

III. Sensorless Position Tracking

The rotor position is estimated during tests #2 and #3 for tracking the *d* and *q* directions in real-time, and avoid position error during the identification.

Position estimation is obtained here by injecting an additional HF voltage signal to the motor windings and demodulating their current response. A position error signal is obtained, and this is forced to zero through a tracking loop. Such saliency-based sensorless techniques are popular for sensorless control at standstill and differ one from the other mainly for the type of injected signal and for the demodulation algorithm. The square wave-voltage method proposed in [13] permits to increase the frequency of the injected signal up to half the switching frequency, and decouple as much as possible the voltage and current signals content related to position estimation from the one related to flux maps identification. Fig. 1 summarizes the block control scheme used for test #2, as an example. For test #3, the control scheme is similar, with both the axes excited using a hysteresis controller. As in most of the literature, also in [13] the HF pulsating voltage is injected along the estimated $\hat{d}$ axis, and the error signal is obtained by demodulating the HF current response on the estimated $\hat{q}$ axis, as shown in Fig. 1. Neglecting the cross-saturation effect, the position error signal is:

$$i_{\hat{q}h} = \frac{u_c(L_d - L_q)}{4\omega_c L_d L_q} \sin(2\Delta\theta) \cong k_\varepsilon \cdot \Delta\theta \tag{3}$$

$$k_\varepsilon = \frac{u_c(L_d - L_q)}{2\omega_c L_d L_q} \tag{4}$$

Where $i_{\hat{q}h}$ is the HF component of $i_{\hat{q}}$ after band-pass filter and demodulation process, u_c the injected voltage amplitude, ω_c the injection frequency, L_d and L_q are differential inductances and $\Delta\theta = \theta - \hat{\theta}$ is the position estimation error. It must be pointed out that this position estimation technique may suffer for error due to cross-saturation [14], especially for high anisotropy motors. However, to correct such error the knowledge of the flux maps would be necessary, that is impossible at this stage.

Back to the benefits on self-commissioning, the on-line estimation of the rotor position permits to track the direction of the estimated $\hat{d}\hat{q}$ reference frame even after eventual small rotor movements. This extends the measurement area in the current plane and makes the identification session much more stable.

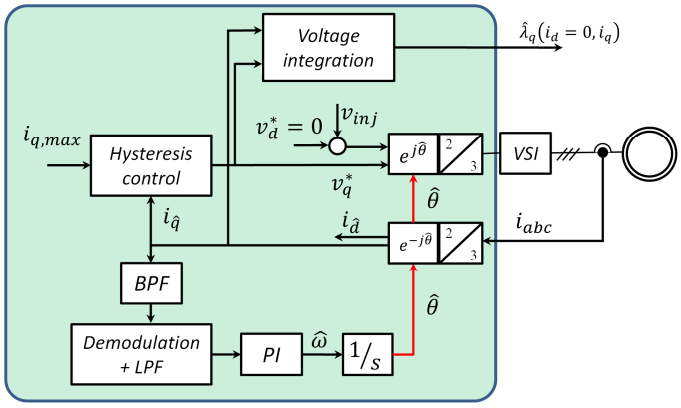

Fig. 1. Block diagram of drive controller configuration used for Test #2, the q axis flux characteristic is measured with $i_d = 0$, with HF injection on d axis.

A. *Tuning of the tracking loop bandwidth*

In this section, guidelines for an appropriate tuning of the position tracking loop are discussed. This is a critical issue of the proposed technique, since an accurate tuning would require the knowledge of the motor flux maps, that is not available before the self commissioning procedure. The equivalent transfer function of the position tracking loop is shown in Fig. 2, where ω_f is the cut-off frequency of the demodulation filter.

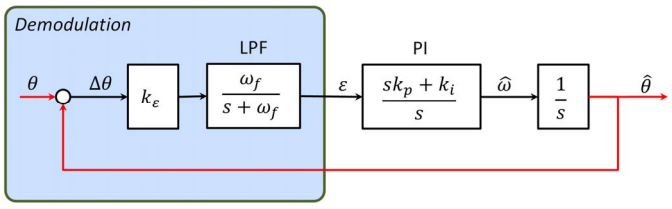

Fig. 2. Sensorless position tracking loop.

For sensorless control, it is usually desired to increase the position estimation bandwidth ω_b as far as possible, in order to have a fast control response in transient conditions. Anyway, in the proposed self commissioning procedure, the rotor movement in test #2 and #3 can be seen as a slow drift from the initial position plus fast vibrations due to the sign variation in the test square wave voltage used for flux identification. The goal of the HF tracking loop is to update the rotor position in order to follow the drift, which is relatively slow, while it is not required to track the vibrations. Therefore, a low bandwidth sensorless control is sufficient (e.g. $\omega_b = 10 \div 20$ rad/s).

B. *Injected voltage amplitude*

Second, it is necessary to evaluate an appropriate value for the injected voltage u_c. A high u_c gives a more clear demodulated signal and therefore the position tracking loop became more stable. Anyway, a high u_c limits the available fundamental test voltages $V_{test,d}$ and $V_{test,q}$, that was demonstrated to improve the test stability and accuracy [12]. During test #2, the voltage vector moves in the angles of a rectangle ($v_d = \pm u_c$; $v_q = \pm V_{test,q}$), while in test #3 it can move in 8 points in the dq plane ($v_d = \pm V_{test,d} \pm u_c$; $v_q = \pm V_{test,q}$). The movement of voltage vector in the v_d, v_q plane is represented in Fig. 3. Taking into account the inverter voltage limitation V_{max}, the following relations hold:

$$u_c < \begin{cases} \sqrt{V_{max}^2 - V_{test,q}^2} & test\ 2 \\ \sqrt{V_{max}^2 - V_{test,q}^2} - V_{test,d} & test\ 3 \end{cases} \quad (6)$$

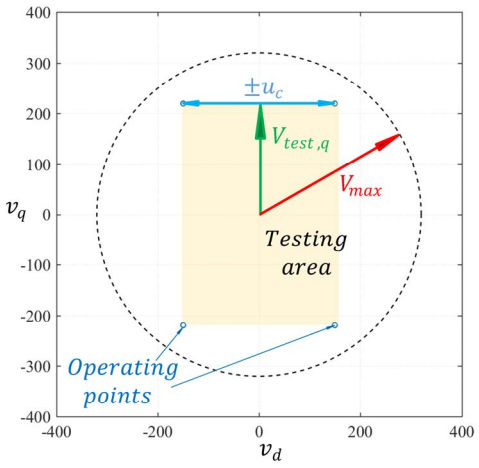

a)

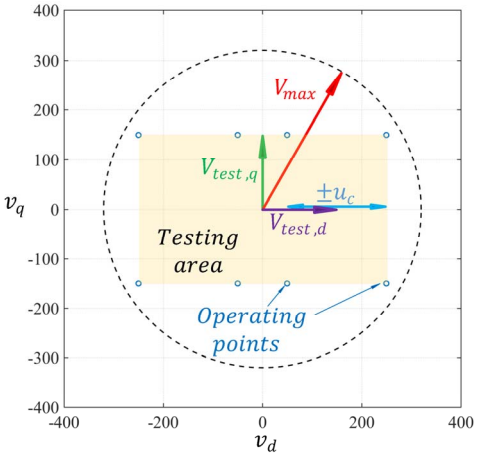

b)

Fig. 3. Testing area for tests augmented with HF injection and inverter voltage limit in $v_d v_q$ plane. a) test #2, $V_{test,q}$=220V, u_c= 150 V, v_{max} = 320 V; b) test #3, $V_{test,d}$=$V_{test,q}$150 V, u_c= 100 V, v_{max} = 320 V.

C. Position error gain

Once determined u_c, the parameter k_ε (4) must be estimated, but this requires a preliminary evaluation of the machine's differential inductances. The value of L_d can be obtained from test #1 which, as said, is always stable and does not require HF injection. Test #2 performed at open loop is marginally stable, but gives enough information for a rough estimation of L_q, useful for tuning the position estimation loop.

According to Fig. 2, the open loop transfer function between the observed and real position is:

$$H = k_\varepsilon \frac{\omega_f}{s+\omega_f} \cdot \frac{sk_p+k_i}{s} \cdot \frac{1}{s} \tag{7}$$

Therefore, neglecting the integrative gain, the bandwidth of the position tracking loop is:

$$\omega_b = k_\varepsilon k_p \tag{8}$$

This last relationship can be used to tune the parameter k_p, after the desired bandwidth value. Afterwards, the integral gain k_i is calibrated considering that the frequency of the zero introduced by the PI regulator must be lower than the bandwidth, for the sake of keeping the phase margin of the tracking loop above 45°:

$$k_i < k_p \omega_b \tag{9}$$

Last, the frequency of the demodulation filter ω_f must be sufficiently higher than the bandwidth but lower than the injection frequency ω_c. The choice of injecting the HF signal at half of the switching frequency permits the highest possible frequency range for the tuning of ω_f and ω_b, therefore it facilitates the tuning procedure in absence of flux maps. In this implementation, the selected values are $\omega_b = 20\ rad/s$, $\omega_f = 940\ rad/s$ and the switching frequency is $f_{sw} = 10\ kHz$.

D. Effects of the HF disturbance on the estimated flux

As can be seen in Fig. 1, the reference voltage signals used for flux estimation are sampled before injection of the HF stimulus u_c, so the voltage integration does not see such component. On the other hand, the measured current is directly used in (1) and (2) without any filtering and therefore it presents an HF oscillation. Anyway, the current contribution to the output of (1) and (2) is minor, so the HF disturbance only produces a small oscillation in the estimated flux characteristics. This effect is negligible if compared to other possible sources of error, such as inaccurate resistance estimation or compensation of inverter nonlinear effects, which are however well compensated as addressed [12]. Therefore, even avoiding filtering the current, the flux estimation (1), (2) is almost immune from HF disturbance. Fig. 4 shows the flux characteristic obtained during test #2, comparing the flux directly estimated from (2) (blue line) with the saturation characteristic obtained when the current is preliminary filtered before voltage integration. As can be seen, the two curves are overlapping. Moreover, the oscillation introduced by the HF injection is further mitigated thanks to the fitting procedure used to extrapolate the flux maps, which is described in the next session.

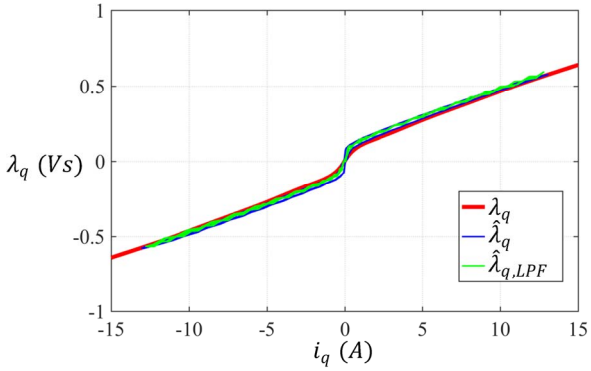

Fig. 4. q-axis saturation characteristic. Red: reference curve measured at constant speed; blue: self commissioning augmented with HFSI; green: self commissioning augmented with HFSI and filtering i_q

IV. Extrapolation of the Flux Characteristic

After the three tests are completed, a post-processing manipulation is necessary to obtain the flux characteristics in a form which is usable for controlling the SyRM drive. For example, the flux maps can be implemented in form of look up tables or, alternatively, using analytical functions. The polynomial magnetic model presented in [11] is based on few parameters and was successfully tested on SyRMs of different size. For this reason it will be used also in this work. The model is based on the following equations:

$$i_d = \lambda_d \left(\mathrm{a}_{d0} + \mathrm{a}_{dd} \lambda_d^S + \frac{a_{dq}}{V+2} \lambda_d^U \lambda_q^{V+2} \right) \tag{10}$$

$$i_q = \lambda_q \left(\mathrm{a}_{q0} + \mathrm{a}_{qq} \lambda_q^T + \frac{a_{dq}}{U+2} \lambda_d^{U+2} \lambda_q^V \right) \tag{11}$$

The exponents can be fixed according to TABLE II. while the coefficients a_{d0}, a_{dd}, a_{q0}, a_{qq} and a_{dq} can be found through iterative linear least square procedure. In particular, a_{d0} and a_{dd} are obtained from test #1, a_{q0} and a_{qq} from test #2 and a_{dq} from test #3. Details can be found in [11].

V. Experimental Results

The proposed square-wave injection self-identification technique augmented by HF signal injection was experimentally tested on a 2.2 kW SyRM. TABLE I. summarizes the main machine characteristics. A dSPACE 1103 PPC controller board was used for the experiments.

TABLE I. SyR Machine under test specifications

Rated power	2.2 kW
Number of poles	4
Nominal phase voltage	400 V
Nominal phase current	5 A
Nominal Speed	1500 rpm
Rated Torque	14 Nm
Phase resistance	3.5 Ω
Moment of inertia	0.005 $kg.m^2$
Switching frequewncy	10 kHz

A. *Flux maps identification*

As said, test #1 is stable using the open loop position estimate approach, therefore this was done without HF injection. Tests #2 and #3 were performed both with and without HF injection, for the sake of comparison.

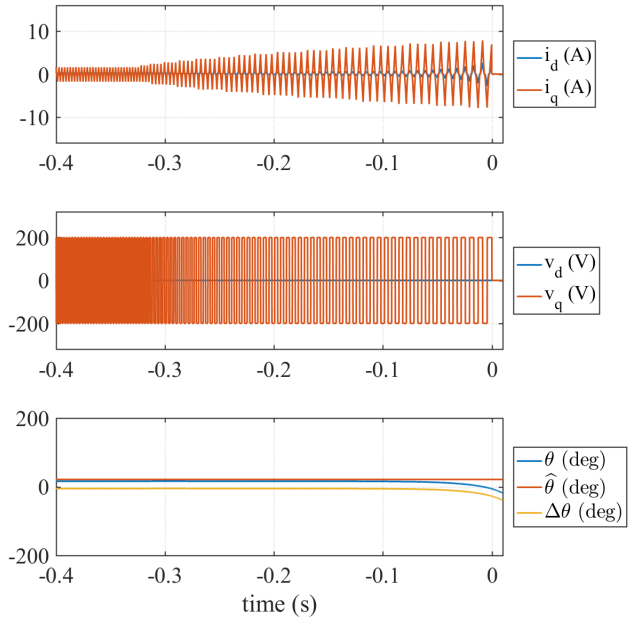

Fig. 5. Test #2 without HF injection. From top to bottom: currents in *dq* axes; applied voltages; measured and observed angle and and position error. $v_{test,q}$ = 200 V.

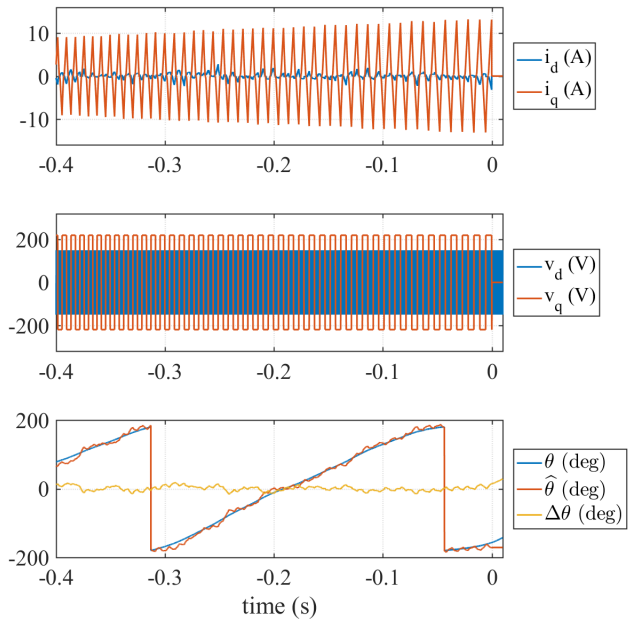

Fig. 6. Test #2 with HF injection. From top to bottom: currents in *dq* axes; applied voltages; measured and observed angle and and position error. $V_{test,q}$= 220 V, u_c= 150 V.

Fig. 5 and Fig. 6 compare the time waveforms of voltages and currents in test #2 where the position is open loop estimated before the test and where the position is closed loop observed through the HF tracking loop, respectively. In both cases, the $i_{q,max}$ limit was progressively increased and the test was stopped when the position error become relevant, according to the stop criterion described in [12]. In Fig. 5, a voltage amplitude $V_{test,q} = 200\,V$ was applied, alone, and the q current reaches a maximum swing of 7.9 A peak. Fig. 6 refers to the same test with HF injection and position estimation. The injected HF voltage u_c was 150 V, the demodulation low-pass filter was set at 150 Hz and the test voltage $V_{test,q}$ was 220 V. From the comparison, it is clear that thanks to the HF position tracking loop the measurement range is considerably improved, since the q current swing was increased from 7.9 A up to 13.2 A peak (+67%).

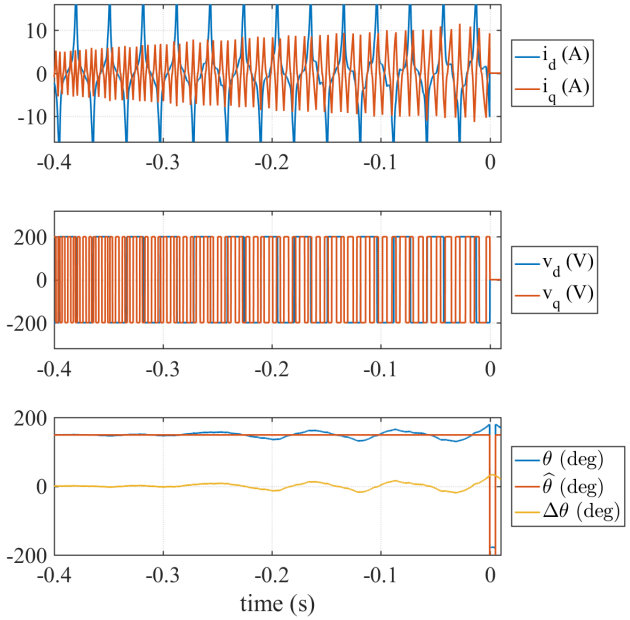

Fig. 7. Test #3 without HF injection. From top to bottom: currents in *dq* axes; applied voltages; measured and observed angle and and position error. $V_{test,d} = V_{test,q}$= 200 V.

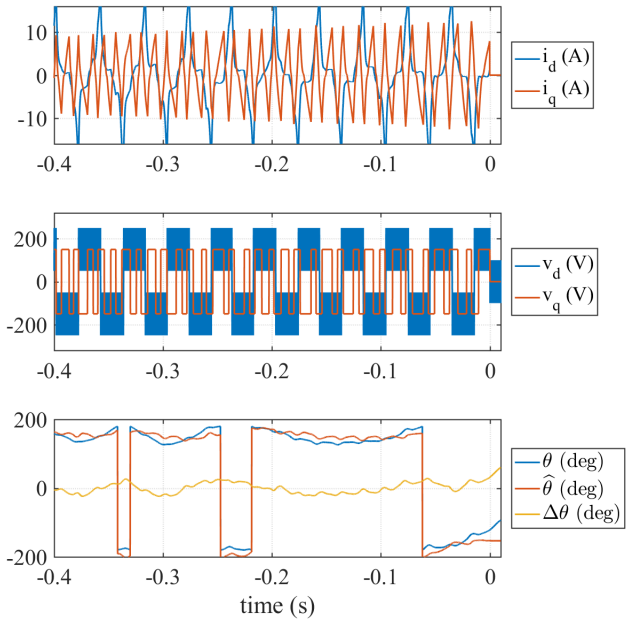

Fig. 8. Test #3 with HF injection. From top to bottom: currents in *dq* axes; applied voltages; measured and observed angle and and position error. $V_{test,d} = V_{test,q}$150 V, u_c= 100 V.

Fig. 7 and Fig. 8 refer to test #3, again comparing the two situations with and without HF signal injection. Also in this case, the $i_{q,max}$ limit was progressively increased, while the $i_{d,max}$ range was kept constant to 20 A. In Fig. 7 the adopted test voltages are $V_{test,d} = V_{test,q} = 200\,V$. In Fig. 8, the injected voltage is $u_c = 100\,V$, the cut-off frequency of the demodulation LPF 50 Hz and the test voltage $V_{test,d} = V_{test,q} = 150\,V$. From the comparison it is evident that, using the same $i_{d,max}$ limit, the $i_{q,max}$ range is marginally improved from 11.5 A to 12.6 A.

These considerations are summarized in Fig. 9, which represents the trajectories covered during the three tests in the dq current plane, with (subfigure a) or without (subfigure b) HF signal injection and position estimation. It is demonstrated that the position tracking increases the stability of tests #2 and, limitedly, #3, so improving the current domain of the identification.

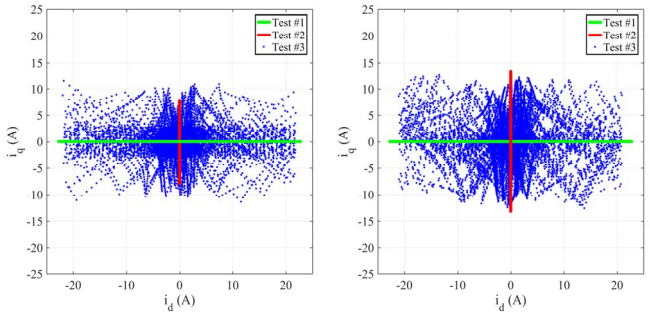

a) b)

Fig. 9. Achievable measurement area in the current plane for test #1, #2 and #3 using open loop using a) open loop position estimation, b) HF tracking loop. Green: test #1; Red: test #2; Blue: test #3.

B. LLS fitting

The LLS procedure described in [11] was used to find the parameters of the analytical algebraic model (10),(11). Optimal values of a_{d0} and a_{dd} were conveniently obtained based on test #1 performed at open loop. Different sets of values for a_{q0}, a_{qq} and a_{dq} were calculated from the results of test #2 and test #3 performed with open-loop position estimation and with the proposed closed-loop position estimation strategy. The parameters obtained in the two cases are summarized in TABLE II.

TABLE II. PARAMETERS OF THE ANALYTICAL MODEL

	a_{d0}	a_{dd}	a_{q0}	a_{qq}	a_{dq}	S	T	U	V
Open loop	2,41	1,47	6,32	41,31	21,96	5	1	1	0
HF injection			13,45	16,86	7,93				

C. Results for test #2

The magnetic curve resulting from test #2 is shown in Fig. 10, where the blue line is the reference model, obtained with the constant speed method, the red line is obtained with open loop position estimation and the green line with HF injection. The saturation characteristic obtained at open loop well represents the reference line up to roughly 8 A, i.e. within the current swing that was explored during the identification. However, the deviation from the reference model is large for higher current values, i.e. in overload conditions. On the other hand, the flux characteristic obtained exploiting the HF injection is well in accordance with the reference up to 15-18 A, thanks to the extended measurement range.

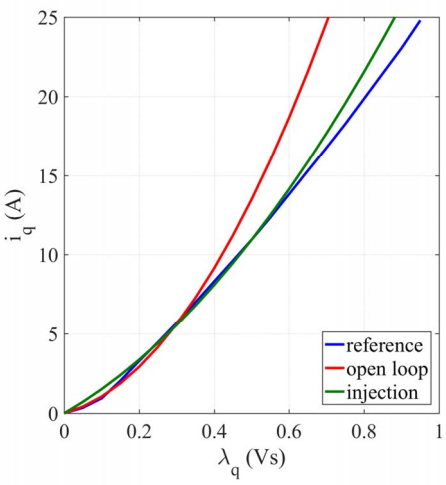

Fig. 10. q-axis saturation characteristic obtained with LLS fitting procedure. Blue: reference curve; Red: test #2 with open loop position estimation; Green: test #2 with position tracking loop.

D. Results for test #3

The results of the LLS fitting procedure based on test #3 are shown in Fig. 11 and Fig. 12, where the same color conventions of Fig. 10 were adopted. Here, the solid lines represent the flux characteristic in each axis when the current in the other axis is null, while the dotted lines are the flux curves in presence of cross-saturation effect. In Fig. 11, $i_d(\lambda_d, \lambda_q = 0)$ curves obtained in the three cases are well superimposed. Conversely, the $i_d(\lambda_d, \lambda_q = 0.6)$ curve is more accurate when obtained from the open loop test (red curves) rather than using HF injection. Therefore, it is evident that the small increase of the measurement area in test #3 obtained using HF injection does not helped improving the cross-saturation evaluation accuracy.

Looking at Fig. 12, the $i_q(\lambda_d = 0, \lambda_q)$ and $i_q(\lambda_d = 1.2, \lambda_q)$ curves are better represented when the HF injection is adopted. The red curves suffer from the error due to the q-axis self-characteristic obtained in test #2 (parameters a_{q0} and a_{qq}), even if the cross-saturation parameter a_{dq} evaluated in test #3 is probably more accurate than the one used for drawing the green curves.

TABLE III. summarizes the suggested testing sequence for the full characterization of the flux maps. It is suggested **to use the HF injection to improve test #2**, and **not to use it during test #3**, which showed to better perform at open loop,

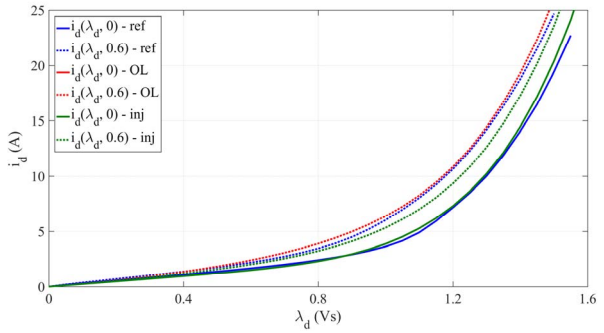

Fig. 11. $i_d(\lambda_d, \lambda_q)$ saturation characteristic obtained after LLS fitting procedure. Blue: reference curve; Red: test #2 with open loop position estimation; Green: test #2 with position tracking loop. Solid lines: $\lambda_q = 0$; dotted lines: $\lambda_q = 0.6$ Vs (strong cross-saturation)

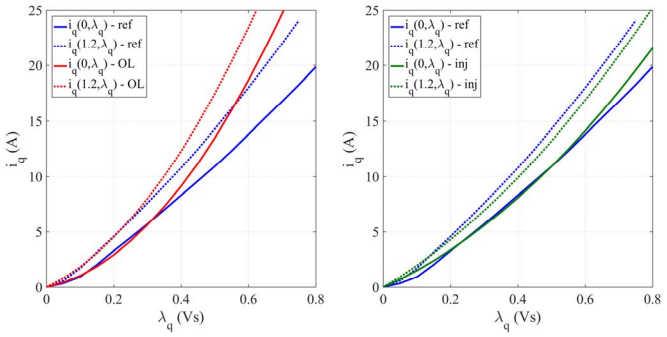

Fig. 12. $i_q(\lambda_d, \lambda_q)$ saturation characteristic obtained with LLS fitting procedure. Blue: reference curve; Red: test #2 with open loop position estimation; Green: test #2 with position tracking loop. Solid lines: $\lambda_d = 0$; dotted lines: $\lambda_d = 1.2$ Vs (strong cross-saturation)

TABLE III. SUGGESTED TESTING PROCEDURE

	open loop	**HF injection**
Test #1	Evaluate $\mathbf{a_{d0}}$, $\mathbf{a_{dd}}$ (Fig. 11)	Not necessary
Test #2	Evaluate L_q for tuning the HF tracking loop	Evaluate $\mathbf{a_{q0}}$, $\mathbf{a_{qq}}$ (Fig. 10)
Test #3	Evaluate $\mathbf{a_{dq}}$ (Fig. 11)	Not necessary

E. Application to sensorless control of the SyR Machine

As proof of concept, the SyRM is controlled using the sensorless control technique presented in [15] associated to the flux curves coming from the self-commissioning. At high speed, the rotor position is model based estimated exploiting active flux concept. A combination of model based and a saliency based tracking loop is used at low speed to achieve high position estimation bandwidth. The saliency based tracking loop imply HF pulsating voltage injection in the estimated $\hat{d}$ axis, while a manipulation of the current in $\hat{q}$ axis is demodulated and used as error signal, in order to compensate position errors due to cross-saturation effects. The motor control algorithm is implemented using Direct Flux Vector Control (DFVC). Flux maps are a key building block of the flux and position observer, mainly for the zero and low speed operating ranges.

For this test, a slow triangular torque reference was imposed to the machine when torque controlled, up to 21 Nm (150 % of the rated value). A driving machine controlled zero speed and a torque meter was used to accurately measure the shaft torque. The test was repeated two times: first using the reference flux maps and then using the saturation characteristics obtained from the proposed self-commissioning technique augmented by HF injection. As can be seen in Fig. 13, the torque tests obtained with the two methods are strictly compatible, proving the validity of the self-identification technique.

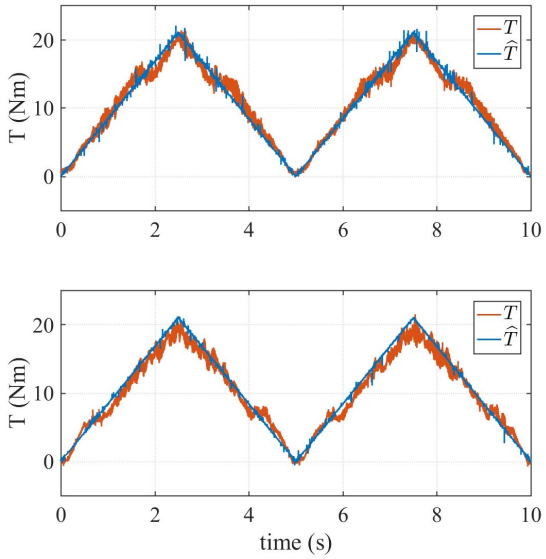

Fig. 13. Torque control tests using reference flux maps (upper) and the flux maps obtained with the proposed self commissioning augmented with HF injection (lower). Blue: observed torque; Orange: measured torque.

VI. CONCLUSIONS

The flux map identification proposed in [11] was augmented by introducing a position sensorless tracking loop that involves HF voltage injection at half of the switching frequency. This allowed to extend the measurement range and stability of test #2, where the q-axis saturation characteristic is evaluated. A slight improvement of the measurement area of test #3 (cross-saturation effect) was also achieved, but without significant effect on the obtained flux characteristic. LLS procedure was used to obtain the parameters of a simple but accurate algebraic model, both for the tests with and without HF position tracking loop. Finally, the flux maps obtained in the two cases were used to implement a sensorless control of the motor under test, proving the goodness of the method and its validity for sensorless control in industrial applications.

REFERENCES

[1] Tuovinen, T.; Hinkkanen, M., "Adaptive Full-Order Observer With High-Frequency Signal Injection for Synchronous Reluctance Motor Drives," in Emerging and Selected Topics in Power Electronics, IEEE Journal of , vol.2, no.2, pp.181-189, June 2014.

[2] Villet, W.T.; Kamper, M.J.; Landsmann, P.; Kennel, R., "Hybrid position sensorless vector control of a reluctance synchronous machine through the entire speed range," in Power Electronics and Motion Control Conference (EPE/PEMC), 2012 15th International , vol., no., pp.LS4b-1.1-1-LS4b-1.1-7, 4-6 Sept. 2012.

[3] E. Armando, R. I. Bojoi, P. Guglielmi, G. Pellegrino and M. Pastorelli, "Experimental Identification of the Magnetic Model of Synchronous Machines," in IEEE Transactions on Industry Applications, vol. 49, no. 5, pp. 2116-2125, Sept.-Oct. 2013.

[4] S. A. Odhano, R. Bojoi, Ş. G. Roşu and A. Tenconi, "Identification of the Magnetic Model of Permanent-Magnet Synchronous Machines Using DC-Biased Low-Frequency AC Signal Injection," in IEEE Transactions on Industry Applications, vol. 51, no. 4, pp. 3208-3215, July-Aug. 2015.

[5] D. Uzel and Z. Peroutka, "Optimal control and identification of model parameters of traction interior permanent magnet synchronous motor drive," in Proc. IEEE IECON 2011, Melbourne, Australia, Nov. 2011.

[6] S. Ebersberger and B. Piepenbreier, "Identification of differential inductances of permanent magnet synchronous machines using test current signal injection," in Proc. SPEEDAM 2012, Sorrento, Italy, June 2012, pp. 1342–1347.

[7] I. Omrane, E. Etien, O. Bachelier, and W. Dib, "A simplified least squares identification of permanent magnet synchronous motor parameters at standstill," in Proc. IEEE IECON 2013, Vienna, Austria, Nov. 2013.

[8] G. Pellegrino, B. Boazzo and T. M. Jahns, "Magnetic Model Self-Identification for PM Synchronous Machine Drives," in IEEE Transactions on Industry Applications, vol. 51, no. 3, pp. 2246-2254, May-June 2015.

[9] B. Stumberger, G. Stumberger, D. Dolinar, A. Hamler and M. Trlep, "Evaluation of saturation and cross-magnetization effects in interior permanent-magnet synchronous motor," in IEEE Transactions on Industry Applications, vol. 39, no. 5, pp. 1264-1271, Sept.-Oct. 2003.

[10] N. Bedetti, S. Calligaro and R. Petrella, "Stand-Still Self-Identification of Flux Characteristics for Synchronous Reluctance Machines Using Novel Saturation Approximating Function and Multiple Linear Regression," in IEEE Transactions on Industry Applications, vol. 52, no. 4, pp. 3083-3092, July-Aug. 2016.

[11] M. Hinkkanen; P. Pescetto; E. Molsa; S. E. Saarakkala; G. Pellegrino; R. Bojoi, "Sensorless self-commissioning of synchronous reluctance motors at standstill without rotor locking," in IEEE Transactions on Industry Applications , vol.PP, no.99, pp.1-1.

[12] P.Pescetto, G. Pellegrino, "Sensorless Standstill Commissioning of Synchronous Reluctance Machines with Automatic Tuning," in proc. IEEE IEMDC 2017, Miami, Florida, May 2017.

[13] Y. D. Yoon, S. K. Sul, S. Morimoto and K. Ide, "High-Bandwidth Sensorless Algorithm for AC Machines Based on Square-Wave-Type Voltage Injection," in IEEE Transactions on Industry Applications, vol. 47, no. 3, pp. 1361-1370, May-June 2011.

[14] P. Guglielmi, M. Pastorelli and A. Vagati, "Impact of cross-saturation in sensorless control of transverse-laminated synchronous reluctance motors," in IEEE Transactions on Industrial Electronics, vol. 53, no. 2, pp. 429-439, April 2006.

[15] A. Yousefi-Talouki; P. Pescetto; G. Pellegrino; I. Boldea, "Combined Active Flux and High Frequency Injection Methods for Sensorless Direct Flux Vector Control of Synchronous Reluctance Machines," in *IEEE Transactions on Power Electronics* , vol.PP, no.99, pp.1-1.